Chapter

Optical Gas Sensors Using Terahertz Waves in the Layered Media

Borwen You and Ja-Yu Lu

Abstract

Terahertz (THz) wave propagation in the layered media is presented based on the waveguide and artificial-material configurations to sense the gas molecules. The single dielectric layer with a cylindrical conformation works as a pipe waveguide in the wave frequency of 0.1–1 THz. For a long-distance propagation over 10 cm of the pipe, resonant modes are characterized from the transmission power dips. The pipe-waveguide resonator works for a THz refractive-index sensor when the resonance frequency is monitored to sense vapor molecules inside the pipe core. Besides of the waveguide configuration, a multilayer microporous polymer structure (MPS) is considered an artificial material to transmit THz waves for sensing gaseous molecules. The MPS is not only transparent to THz waves but also enhances the detection resolution of THz absorption for the vapor molecules. The porous structure provides a large hydrophilic surface area and numerous micropores to adsorb or fill vapors, thereby leading to greatly enhanced wave-analyte interaction with an apparent THz signal change. Different concentrations of toxic methanol adulterated in alcoholic aqueous solutions are thus identified in their vapor phases by using the MPS-based THz sensor.

Keywords: terahertz wave, optical sensor, waveguide, terahertz spectroscopy, polymers, multilayers, and fiber optics sensor

1. Introduction

Gas sensing for pollutant monitoring and leaky molecules detection is important when the environmental issues on breath health are revealed. Various gas sensors based on different principles are presented, such as the gas chromatography-mass spectroscopy [1–3], electrochemical [4], and optical sensors. For the electrochemical sensors [5, 6], the high sensitivity is requested from the high operation temperature, which is risky for explosive gas detection due to the high-power consumption at electrodes. The optical sensing scheme can solve the unsafe problem because of the room-temperature operation without electric contact [7–9]. THz radiation, which lies between the infrared ray (IR) and microwave regions, can strongly perturb polar gas molecules with the energy level transitions of rotation or vibration. The absorption strength of gas molecules in the THz frequency range is typically on the same order of magnitude as the IR region, and is $\sim 10^3$–10^6 stronger than that in the microwave region [10]. The low photon energy of the THz wave is

relatively safer than that of IR wave and has the stronger interaction response than that in the microwave region [11–13].

THz gas sensing methods have been demonstrated based on two main styles. The first style is normally illuminating THz radiation directly on the gaseous analytes and acquiring their spectral response for the sensing purposes. For example, the strong absorption lines at specific frequencies (i.e., fingerprint spectra) or the pulse power decay within one certain THz spectral width have been applied to analyze the gaseous analytes [14]. Such the sensing performance are presented from the photo-mixing [15], heterodyne detection [3, 16], and chirped-pulse THz spectroscopy [12]. Such the spectroscopic systems successfully analyze the gas mixtures of more than 30 chemicals [3] and distinguish gases that possess similar compositions. This recognition scheme provides high selectivity based on the rotational/vibrational transition of gas molecules. Nevertheless, the THz spectroscopic system should be equipped with a long gas cell [3, 12, 14], a cryo/sorbent pre-concentration system, and a heating apparatus [3, 16] to improve the sensing limit from the ppm concentration to the ppb level. The overall configuration is complicated, bulky, expensive, and consumes high power. Although the quantum cascade laser is presented as a compact THz laser source for gas sensing applications to simplify THz wave generation [17]. However, the THz laser source should be operated in the low-temperature condition and is limited for practical applications.

The other method of THz gas sensing is to use the THz resonance field in the photonic or periodic structures [18, 19]. For example, one- and two-dimensional photonic structures respectively based on the silicon slabs [18] and pillar arrays [19] have been validated for the non-specific gas sensing in the THz frequency range. The proposed photonic structures have high-quality factors on THz field resonance and are sensitive to slight changes of refractive index. The demonstrated detection limit for hydrogen gas is about 6% concentration change [18]. The approved minimum detectable amount of oxygen or argon is ~1 μmol [19]. Although the resonator-type THz gas sensor is relatively compact, portable, and consumes low power, its short interaction length inside the chip essentially leads to the limited sensitivity and poor selectivity.

In this chapter, THz gas sensors with sufficiently long interaction lengths are presented based on THz wave propagation along the dielectric layers. The layered media specifically perform the enhancement of THz resonance and absorption in the dielectric waveguides and porous structures, respectively. The interaction between THz wave and gas analytes thus becomes efficient. The presented waveguide sensor contributes the detection of THz refractive index variation based on the resonator principle of Fabry-Pérot (FP) etalon, and the porous structures detect vapor molecules based on the response of molecular dipole moment for THz wave absorption.

2. Gas sensors based on THz refractive-index detection

2.1 Pipe-waveguide resonator

One dielectric layer bent to be a cylindrical structure can be used as one hollow core waveguide to guide THz waves. Those dielectric pipes or tubing used for THz pipe waveguides are available from the hydroelectric materials and demonstrated in the literatures [20]. In the study, a 30 cm-long glass pipe is used to load 0.05 cm^3 liquid analytes to evaporate and fill the pipe core. When THz waves input and pass through the glass-pipe core, the vapor molecules interact with the THz wave for the sensing purpose.

The cylindrical layer acts as a FP etalon, and THz waves satisfying the FP resonance condition enables field resonance inside the cylindrical layer, which becomes leaky to form multiple transmission dips. Based on the FP criteria, the resonant wavelength of THz waves in the cylindrical layer is defined as, $\lambda_m = 2d\sqrt{n_{cld}^2 - n_{cor}^2}/\mathrm{m}$, where λ_m, d, m, n_{cld}, and n_{cor} are, respectively, the m$^{\mathrm{th}}$-order resonant wavelengths, thicknesses of a cylindrical layer, orders of the resonant modes, and effective waveguide refractive indices of cylindrical layer and the pipe core [21]. **Figure 1** shows the transmission spectrum of a blank glass pipe, where the spectral dips with low power represent the FP resonant waves along the glass layer. The measured resonant frequencies are approximate to the calculated results via finite-difference time-domain (FDTD) method. The cross section of the glass-pipe sensor is shown in the inset of **Figure 1**, where the inner core diameter D_{in} and the thickness of pipe-wall are 5.57 and 1.17 mm, respectively. The refractive indices of the air-core and glass used in simulation are 1 and 2.6 [17], respectively. There are five spectral dips of the glass-pipe waveguide in the transmission spectrum, 0.2–0.5 THz (**Figure 1**), which are 0.201, 0.266, 0.326, 0.392 and 0.452 THz frequencies. According to resonance condition of FP etalon, the resonant dip frequency changes with n_{cor}, and thus various vapors can be identified in the hollow core by detecting the spectral shifts of the resonant dips.

THz resonant fields inside the cylindrical layer must be sufficiently evanescent toward the air core to make the pipe-waveguide resonator sensitive to the vapor molecules. Interaction between the THz resonant field and the vapor molecules is therefore enhanced, consequently resulting in the sensitive detection. Based on the investigation of THz dielectric pipe waveguides, the high order resonance waves have strong evanescent field inside the pipe core [22]. That is, the resonance dips at the high frequency range have stronger core field than those at the low frequency range. The resonant dip at 0.452 THz as shown in **Figure 1** is thus suitable to probe vapors within the glass pipe core because of the powerful resonant field to interact vapor molecules.

2.2 Vapor sensing principle and results

To approve the sensing principle of a pipe waveguide sensor, the vapor molecules of the water, hydrochloric acid (HCl), acetone and ammonia liquids are used

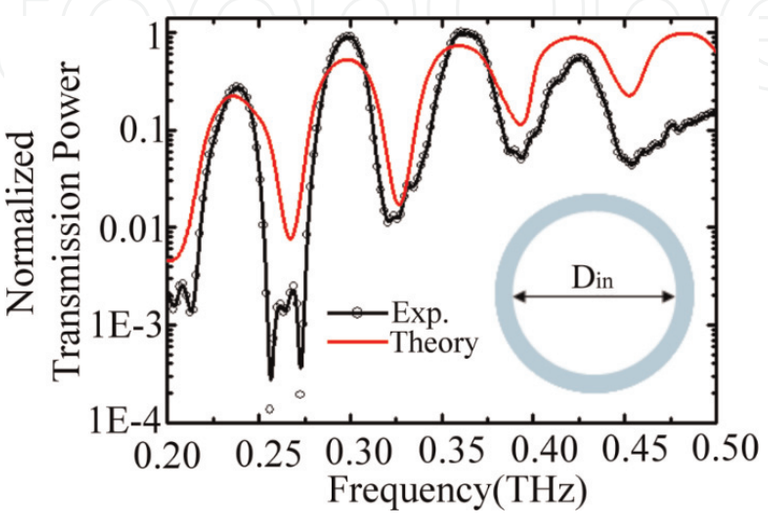

Figure 1.
Transmission spectra of a glass-pipe waveguide: (inset) the cross section of a glass-pipe-waveguide sensor (reprinted from Opt. Express 20, 5858-5866 (2012). © 2012 OSA.

as the standard analytes. The sensing results show that the spectral dip of 0.452 THz obviously shifts toward the high frequency range when various vapors fill in the pipe core (**Figure 2a**). The spectral dip position is shifted to 0.461, 0.465 and 0.477 THz, respectively, for the HCl, acetone and ammonia vapors. Based on the measured spectral dips and FDTD calculation method (**Figure 2b**), the related effective refractive indices of the pipe core ($n_{eff.core}$) are obtained as shown in **Figure 2c**. The core indices of the glass pipe are 1.016, 1.035 and 1.102 for the vapors of HCl, acetone and ammonia, respectively (**Figure 2c**).

The dip-frequency-shift only occurs at the resonance dip of 0.452 THz and the other resonance dips in the low-frequency range do not exhibit any spectral shift for sensing the vapors, which is different from the calculated results in **Figure 2b**. The zero spectral-shift for the low-frequency-dips comes from the low strength of leaky resonance field at the pipe core. It is too weak to sense the presence of vapor molecules. This performance implies that the resonant fields for detecting vapors in the pipe core require high transmission power to identify slight core-index variation for the low densities of vapors. This low sensitivity phenomenon without any significant spectral shift is straightforward correlated to all the anti-resonant fields, i.e., the spectral peaks at the frequency lower than 0.52 THz.

Figure 2c shows the relation between the spectral dip frequencies and the $n_{eff.core}$ values for different vapors inside the pipe core. The dip frequencies increase with the $n_{eff.core}$ values. The increment effect of $n_{eff.core}$ arises from the various vapor pressures of the volatile liquids, which are generated from the 0.05 cm^3 liquid volume. High vapor pressure represents large amounts of vapor molecules inside the pipe core. Therefore, the vapor pressures of volatile liquids are approximately proportional to the quantities of vapor molecules in the sealed pipe core. The high density of the vapor molecules in the pipe core results in the large $n_{eff.core}$, and the resonant dip of 0.452 THz has an apparent blueshift.

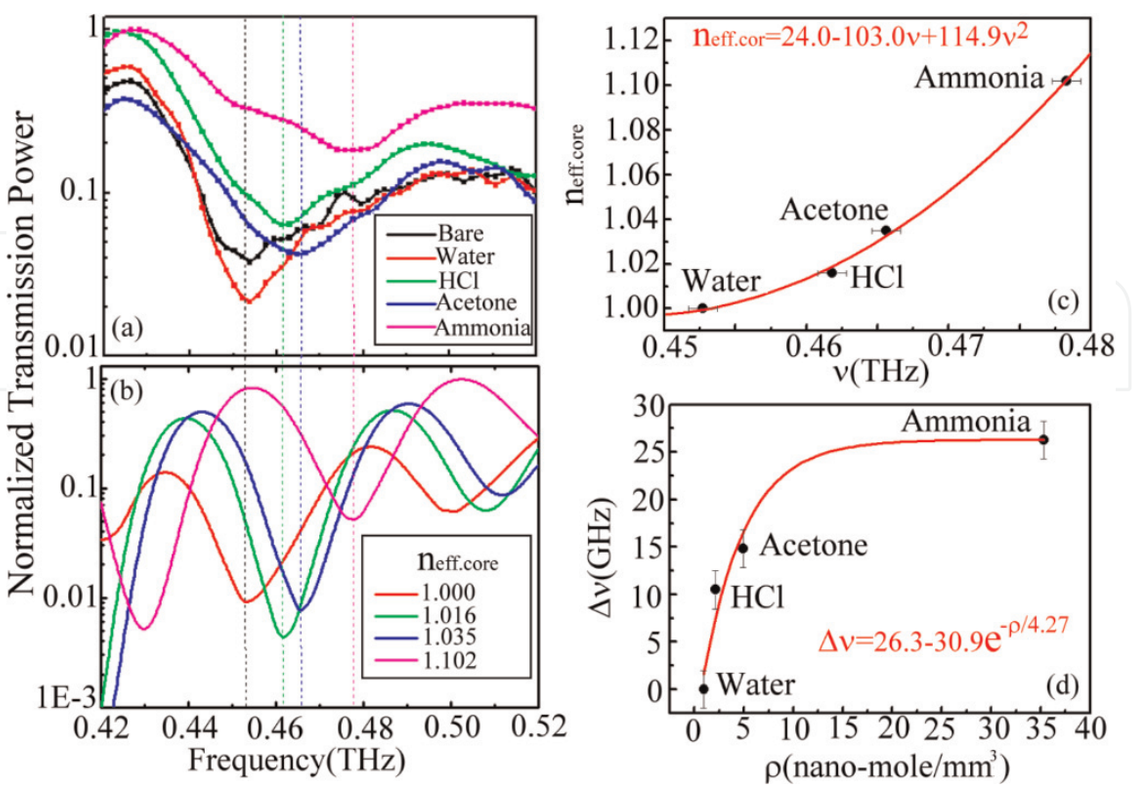

Figure 2.
The spectral dip shift of (a) sensing results and (b) FDTD calculation for different vapors. (c) Relation between $n_{eff.cor}$ *and ν for different vapors. (d) Relation between spectral dip shift and the estimated vapor densities (reprinted from Opt. Express 20, 5858-5866 (2012). © 2012 OSA).*

The $n_{eff.cor}$ value versus the resonance frequency can be fit by curve of $n_{eff.cor} = 24 - 103\nu + 114.9\nu^2$ (**Figure 2c**). The slight index variation could thus be estimated via this fitting cure to identify the molecules in the pipe core. However, the water analyte in the pipe core cannot contribute any spectral shift because the density of water vapor is quite low. The sensing result is reasonable because the vapor pressures of water, HCl, acetone and ammonia at normal atmosphere and room temperature are, respectively, around 17 [23], 38 [24], 202 [24] and 308 [23] mm-Hg.

For qualitative analysis, the vapor molecules discussed in this work are assumed as the ideal gases and their densities in the enclosed pipe would be calculated based on the ideal gas law. **Figure 2d** illustrates the relation of molecular density (ρ) and spectral dip shift ($\Delta\nu$), which can be fit as $\Delta\nu = 26.3 - e^{-\rho/2.7}$. **Figure 2d** illustrates that the blueshift relative to 0.452 THz frequency gradually saturates when the vapor density is over 10 nano-mole/mm^3. The saturation response eventually reduces the sensitivity of the pipe sensor. Based on the spectral resolution of 4 GHz and the fitting curve in **Figure 2d**, the minimum detectable molecular quantity would be around 7.8 μmole, corresponding to a molecular density of 1.6 nano-mole/mm^3.

3. Gas sensors based on THz absorption detection

3.1 Microporous polymer structures (MPSs)

Besides of the single cylindrical layer, multiple layers of MPS can be used as a THz gas sensor. The sensing mechanism of THz wave is monitored from THz absorption of gas molecules, different from the refractive-index detection of the pipe-waveguide resonator. A MPS gas sensor is integrated from multiple layers of polyethylene terephthalate (PET) mesh (SEFAR PET1000, SEFAR AG, Switzerland). To collect and seal the gaseous analytes, MPS is assembled with one microfluidic chamber, which is made of Teflon material. As shown in **Figure 3a** and **b**, a PET mesh is flexible and consists of periodical square holes. PET mesh layers are stacked and fixed by a rectangular acrylic holder to form a MPS structure. There are large numbers of micropores (i.e., square air holes) in one MPS and the micropores are random inside the composite.

Figure 3c shows the schematic diagram of the THz gas sensor based on a MPS device and a microfluidic chamber. The MPS sensor is compact and low loss for THz waves, different from the bulky gas chambers. A flexible plastic tubing to the fluidic

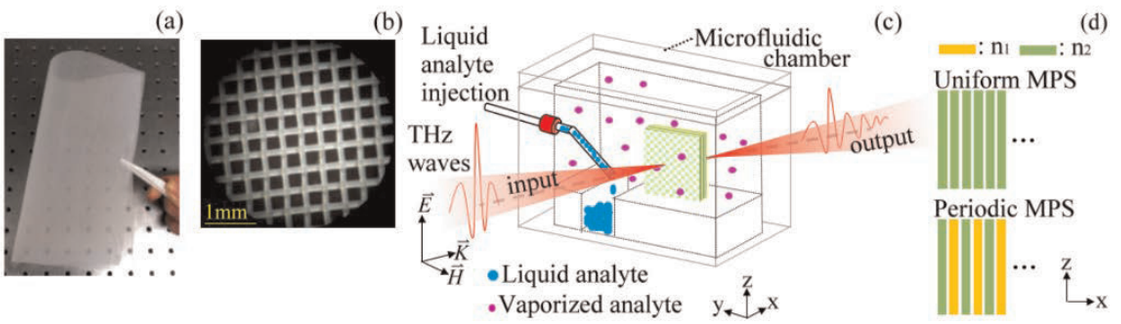

Figure 3.
(a) Macroscopic and (b) microscopic photographs of a PET mesh. (c) The scheme of a MPS volatile gas sensor. (d) Uniform and periodic configurations of the MPSs in the x-z *plane (reprinted from Opt. Express 25, 5651-5661 (2017). © 2017 OSA).*

channel is externally connected with the sample chamber for easy control of the liquid analyte and its vapor. The inner volume of the chamber is larger than the MPS dimension and sealed to easily achieve the saturated pressure of vapor analyte. The inner chamber has a width of 21 mm (x-axis), a length of 60 mm (y-axis), and a height of 45 mm (z-axis). One fluidic channel (18 mm long in x-axis, 5 mm wide in y-axis, and 3 mm deep in z-axis) is machined at the bottom of the Teflon chamber for loading the liquid analytes that are injected via the external tubing. The liquid analytes evaporate, becoming vapors, and diffuse into the MPS. In the volatile gas sensing experiment, the sample loading and sensing processes are performed at room temperature and normal atmosphere without enforcing pump or additional heating process.

To study the sensing performance dependent on the MPS dimensions, four kinds of PET meshes with different thicknesses and square micropore sizes are stacked into two MPS configurations, which are the uniform and periodic structures (**Figure 3d**). The micropores of each PET meshes in a MPS were not precisely aligned with each other when the PET layers are randomly placed layer by layer for both uniform and periodic MPSs. The periodic MPS is constructed by alternately stacking two kinds of PET meshes that have different micropore sizes. In the other way, the uniform MPS is made by stacking only one kind of PET mesh. Different micropore sizes of PET meshes represent different porosities or different effective refractive indices (e.g., n_1 and n_2 in **Figure 1d**). To investigate the pore size effect for the vapor sensitivity, large- and small-pore MPSs are prepared in both the uniform and periodic structures using the four kinds of PET meshes.

In the geometric designs, large-pore periodic MPS is composed by the PET meshes with 90 and 249 μm pore widths, denoted as *Periodic-90-249 MPS*. *Periodic-45-133 MPS* represents the small-pore periodic MPS, possessing 45 and 133 μm pore widths of the PET meshes. Similarly, the small- and large-pore uniform MPSs are denoted as *Uniform-45* and *Uniform-90 MPSs*, respectively. Their pore widths of the composed PET meshes are 45 and 90 μm, respectively. The specifications of the applied MPS devices are list in **Table 1**, including the pore width, mesh thickness, stacking layer number, device thickness, and effective porosity.

MPS No.	Pore width (μm)	PET mesh thickness (μm)	Layer number	MPS thickness (mm)	Effective porosity (%)
Periodic-90-249	249	200	23	3.46	40.5
	90	50			
Periodic-45-133	133	100	6	0.45	37.2
	45	50	34	2.55	
			46	3.45	
Uniform-90	90	100	23	2.3	30.1
Uniform-45	45	50	6	0.3	29.6
			12	0.6	
			34	1.7	

Reprinted from Opt. Express 25, 5651-5661 (2017). © 2017 OSA.

Table 1.
MPS specification.

3.2 Sensing principle

The effective absorption coefficients and refractive indices of MPS micropores are observed in the sensing process to distinguish different types and concentrations of volatile gases. The transmitted power spectra of the microporous structure with and without vapor analytes are defined as follows,

$$P_{v+p}(\omega) = P_0(\omega)e^{-2\alpha_{v+p}(\omega)L}, \tag{1}$$

$$P_p(\omega) = P_0(\omega)e^{-2\alpha_p(\omega)L}. \tag{2}$$

The subscripts p and $v + p$ in the Eqs. (1) and (2) represent the sample chamber without and with vapor analytes, respectively. $P_0(\omega)$, $\alpha(\omega)$, and L mean the power of input THz wave, effect absorption coefficients of micropores, and thickness of the multilayer-stacked device, respectively. Based on the effective medium concept, the effective absorption coefficient of MPS that is defused with vapor analytes can be written as,

$$\alpha_{v+p} = \alpha_v f + \alpha_{PET}(1-f). \tag{3}$$

For the blank structure, the effective absorption coefficient is defined as,

$$\alpha_p = \alpha_{air} f + \alpha_{PET}(1-f). \tag{4}$$

In Eqs. (3) and (4), the factors of f, α_v, α_{air}, and α_{PET} indicate the air filling ratio of micropore volume, the absorption coefficients of vapor analyte, air, and PET material, respectively. α_{v+p} and α_v in Eqs. (1) and (2) are substituted by Eqs. (3) and (4). The absorption coefficient variation $(\alpha_v - \alpha_{air})$ is consequently shown as,

$$\alpha_v - \alpha_{air} = \left[\ln\left(P_p/P_{v+p}\right)\right]/(2fL). \tag{5}$$

The value of $(\alpha_v - \alpha_{air})$ approximates to α_v because the THz wave absorption of air is as small as 10^{-5} cm^{-1} [25]. Thus, the absorption coefficient of vapor (α_v) can be obtained in the approximate condition. The effective medium concept to express the absorption coefficients of the micropore in Eqs. (4) and (5) represents the absorption value within the unit pore space/volume. We thus denote α_{eff} as the vapor absorption coefficient instead of α_v to emphasize the critical assumption of effective medium idea (Eq. (6)).

$$\alpha_{eff} = \left[\ln\left(P_p/P_{v+p}\right)\right]/(2fL). \tag{6}$$

Furthermore, the phase difference for the unit pore volume with and without vapors in the MPS can be defined as $(\Delta\phi/V_{pore})$, where $\Delta\phi = \phi_{v+p} - \phi_p$ and V_{pore} are the phase difference for MPS with-without vapors and the total pore volume, respectively. The phase difference $\Delta\phi$ and the total volume of MPS, V_{pore}, can be individually estimated from Eqs. (7) and (8),

$$\Delta\phi = (\omega/c)\cdot\Delta n\cdot L, \tag{7}$$

$$V_{pore} = A_{beam}\cdot f\cdot L. \tag{8}$$

Δn, ω, c, and A_{beam} are the refractive index variation, angular frequency, light speed in vacuum and input THz beam size on the MPS structure, respectively. The phase difference for the unit volume of micropore is thus presented as,

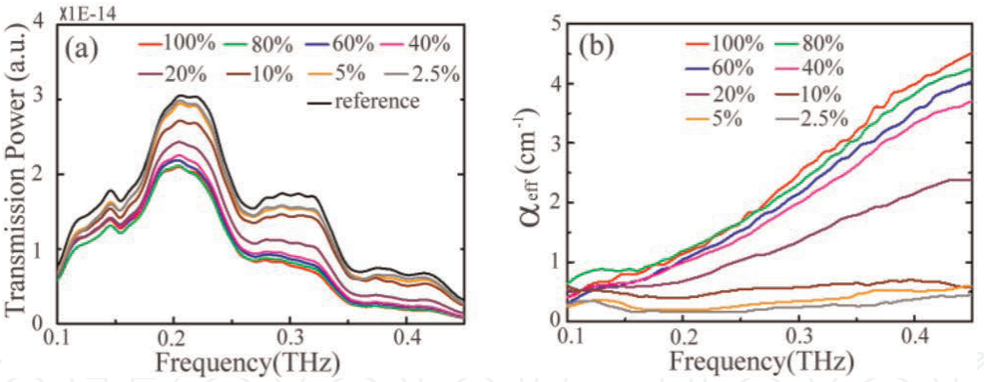

Figure 4.
(a) Power transmission spectra and (b) the corresponding effective absorption coefficient spectra within the unit volume of micropore for various aqueous acetone concentrations (reprinted from Opt. Express 23, 2048-2057 (2015). © 2015 OSA).

$$\Delta\phi/V_{pore} = (\omega/c)\cdot\frac{\Delta n}{(A_{beam}\cdot f)}. \tag{9}$$

Based on Eq. (9), we consider the effective refractive index variation of the unit pore volume, Δn_{eff}, correlating to the macroscopic version of refractive index variation, Δn, as

$$\Delta n_{eff} = \frac{\Delta n}{(A_{beam}\cdot f)}. \tag{10}$$

The macroscopic variation of refractive index (Δn) can be obtained from Eq. (9) as,

$$\Delta n = \frac{c}{\omega}\cdot A_{beam}\cdot f\cdot\frac{\Delta\phi}{A_{beam}\cdot f\cdot L} = \frac{c\cdot\Delta\phi}{\omega\cdot L}. \tag{11}$$

Eq. (10) is then substituted by Eq. (11) and re-written as,

$$\Delta n_{eff} = \frac{c\cdot\Delta\phi}{A_{beam}\cdot f\cdot L\cdot\omega}. \tag{12}$$

The effective refractive index variation within the unit volume of micropore (Δn_{eff}) can eventually be extracted from the phase information of the measured THz waveforms ($\Delta\phi$) and the pore volume that is radiated by the THz-wave beam spot. That is, $V_{pore} = A_{beam}\,L\,f$. Based on the sensing principle as shown in Eqs. (1)–(12), the detected THz fields within the unit pore volume of micropore are measured and compared with and without vapors infiltration in the scheme (**Figure 3c**). Because of the transparent property of PET material in THz frequency, the scattering loss of surface roughness along the propagation axis can be excluded.

3.3 Volatile gas sensing abilities

The *Periodic-90-249 MPS* device was used to study the volatile gas sensing abilities of MPS and observed for the α_{eff} response under different amounts of acetone vapor exposure. **Figure 4a** illustrates THz power transmission spectra of the *Periodic-90-249 MPS* before and after exposure to different concentrations of acetone vapor. The THz spectra are apparently identified for acetone aqueous

solutions with concentrations from 2.5 to 100%. In the sensing scheme (**Figure 3a**), all the acetone aqueous solutions naturally evaporate until the vapor pressure is saturated in the chamber. According to the Raoult's law [26], the aqueous acetone concentration is approximately proportional to the vapor pressure. That is, the large concentration of acetone aqueous solution generates a large acetone vapor pressure. The increased amount of acetone vapor results in power reduction in the THz frequency range of 0.1–0.45 THz (**Figure 4a**).

Figure 4b presents the α_{eff} spectra under different concentrations of acetone vapor exposure, which is extracted from the parameters of spectral transmittance, MPS thickness of 3.46 mm, and the micropore filling ratio, 40.5% (Eq. (6)). The absorption coefficient increases with THz frequency and vapor molecular density. Based on the ideal gas formula and vapor pressures of acetone aqueous solutions, the vapor densities of acetone (ρ) can be obtained. The vapor pressures for different concentrations of acetone solutions are estimated based on the experimental database in [27] and not by using Raoult's law.

THz time-domain spectroscopy (THz-TDS) was used to integrate MPS devices to observe the sensing performance of 0.10–0.45 THz waves. **Figure 4b** shows the extracted α_{eff} values obviously achieve the largest distinction at 0.4 THz. Above 0.4 THz frequency, the signal-to-noise ratio is too low for the vapor sensing. Therefore, we apply the 0.4 THz wave to probe α_{eff} and Δn_{eff} that are responded from the vapor molecules in the MPS devices. Based on the spectroscopic curves of α_{eff} in **Figures 4b** and **5a** and **b** illustrate the sensing results of 0.4 THz wave to detect different concentrations of acetone vapors with and without using the MPS inside the chamber, respectively.

The α_{eff} and Δn_{eff} values of THz wave apparently rise within an acetone vapor density (ρ) of 6 nmol/mm^3 and become saturated while ρ is about 6–14 nmol/mm^3. This trace trends between α_{eff} and Δn_{eff} versus ρ are consistent. It implies that the increased acetone vapor molecules not only significantly absorb the THz wave (represented by α_{eff}) but also introduce considerable phase retardation in the THz electric field oscillation (represented by Δn_{eff}). The high ρ value certainly makes the infiltration of vapor molecules into the micropores and increases the molecular adsorption capacity of the hydrophilic surface [28]. The acetone vapor molecules, confined in the micropores and adsorbed on the pore surface of MPSs, consequently cause the increment of α_{eff} and Δn_{eff}.

The α_{eff} responsivity in **Figure 5a** can be fit by the Langmuir adsorption isotherm with a high R^2 value (>97%). The Langmuir fitting indicates that the monolayer adsorption of acetone vapor molecules on the hydrophilic microporous surface is

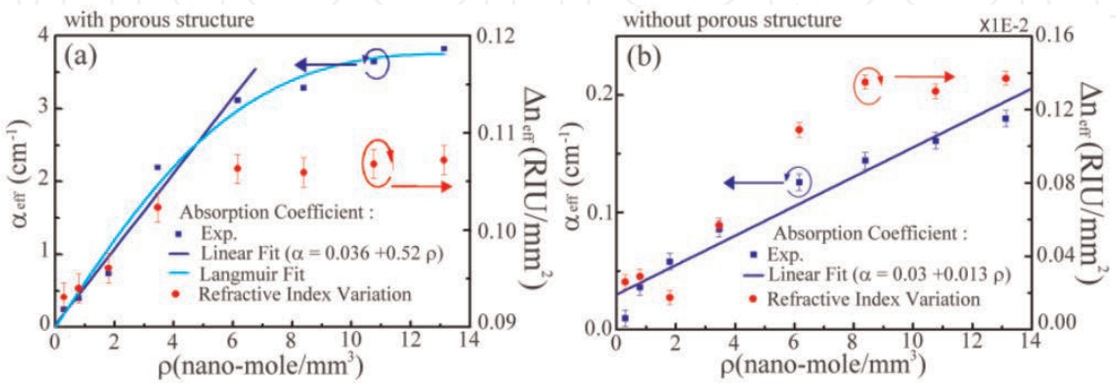

Figure 5.
Detecting the effective absorption coefficients (blue square dot) and refractive index variation (red circular dot) at 0.4 THz for various acetone vapor densities (a) with and (b) without the Periodic-90-249 MPS. *The blue and cyan curves indicate the mathematical fit of the proportional relationship and the Langmuir adsorption isotherm, respectively (reprinted from Opt. Express 23, 2048-2057 (2015). © 2015 OSA).*

mainly caused by physisorption. For the molecular density of <6 nmol/mm^3, the proportional response of the 0.4 THz wave absorption versus the acetone vapor density can be linearly fit as $\alpha = 0.036 + 0.52\rho$ and considered the sensitive region of the sensor, which is denoted by the blue line in **Figure 5a**. The lowest detected concentration of acetone vapor is 291 pmol/mm^3, which is indicated as the first data point of **Figure 5a** and corresponding to 17 ppm. From the slope of the linear fitting curve and α_{eff} inaccuracy (about 0.01–0.02 cm^{-1}), the minimum detectable concentration change of acetone vapor is <108 pmol/mm^3, which is equivalent to 6.29 ppm. Therefore, MPS are particularly advantageous for minute vapor sensing with a detection limit of low ppm level.

Figure 5b shows the sensing results for different ρ values inside the blank chamber without MPS. For the same ρ, the α_{eff} and Δn_{eff} values inside the blank chamber are smaller than those measured with the MPS. The air-filling ratio (f) quals 100% when we obtain α_{eff} and Δn_{eff} for the blank chamber and based on Eqs. (6) and (10). The MPS enhances the THz absorption about 20 times higher than that in the blank chamber (**Figure 5a** and **b**). In addition, the Δn_{eff} in MPS is two orders of magnitude larger than that in the blank chamber for the same ρ. Both α_{eff} and Δn_{eff} slowly increase with vapor density and without the saturation effect for the blank chamber sensing, which is contrast to the MPS condition.

For an acetone liquid concentration of 100% (~13 nmol/mm^3 vapor molecules), the absorption coefficient at 0.4 THz is ~0.18 cm^{-1} in **Figure 5b**, which is on the same order and reasonably agreed with the published value of 0.45 cm^{-1} in [29]. According to the slope of the linear fitting curve in **Figure 5b** and the system uncertainty of α_{eff}, the minimum detectable molecular density variation of acetone vapor is ~0.558 nmol/mm^3, which equals 32.37 ppm. This result reveals that the sensitivity of volatile gas detection by the MPS is higher than that by a traditional THz-TDS system. Given that the MPS can congregate volatile vapors inside the micropores and adsorb on the hydrophilic surface, the interaction strength between THz radiation and polar gas molecules can be enhanced via the adsorbent medium to significantly increase the absorption and index variations.

The sensing ability of MPS is additionally approved to detect other volatile organic compounds (VOCs), including methanol, ethanol, and ammonia. For the three vapors, both the 0.4 THz α_{eff} and Δn_{eff} increase with vapor densities (**Figure 6**). The trends are approximate to the sensing result of acetone vapor (**Figure 5**), but the saturation responses of α_{eff} and Δn_{eff} are different. The *Periodic-90-249 MPS* exhibits obvious differences of α_{eff} and Δn_{eff} among the three VOCs

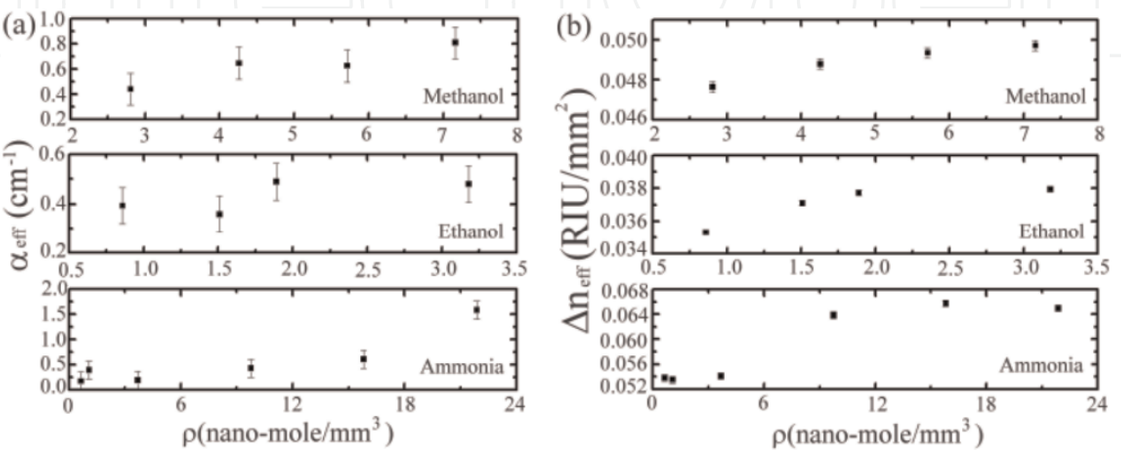

Figure 6.
Detecting (a) effective absorption coefficients and (b) refractive index variations at 0.4 THz for different densities of methanol, ethanol, and ammonia vapors by the Periodic-90-249 MPS *(reprinted from Opt. Express 23, 2048-2057 (2015). © 2015 OSA).*

(**Figure 6**), which are responded from the enhanced adsorption and infiltration of vapors in the micropores. In this sensing configuration of MPS, capillary condensation of vapors does not occur in the micron-sized pores for all vapor species [30, 31].

The 0.4 THz α_{eff} values for different concentrations of acetone, methanol, ethanol, and ammonia vapor exposures are summarized in **Figure 7a**. The magnitude order from the largest to smallest α_{eff} values is ketone, alcohol and ammonia. The linear fitting curves, denoted by the dashed lines in **Figure 7a**, represent the molecular responses of the MPS microporous to the vapor analyte. The sensing ability of MPS is significant to identify the three VOC classes. Each type of vapor has a distinct α_{eff} curve that can be used to distinguish from other vapors. THz radiation can strongly perturb the dipole moment of a VOC, and predominantly induce molecular motion to increase the THz absorption coefficients. Based on the investigation in **Figure 7b**, the magenta columns present magnitudes of the dipole moments of the four polar vapors in the following order: ketone > alcohol > ammonia [32]. The order of molecular dipole moment is approximate to the magnitude sequence of the THz absorption coefficients (**Figure 7a**). The THz interaction strength of acetone vapor is higher than those of the other vapors. Methanol and ethanol vapors belong to alcoholic VOCs and have similar THz absorption coefficients in the MPS. The sensitivities of MPS for detecting the four vapors can be evaluated when considering the linear fitting slopes and the system inaccuracies of α_{eff}. The detection limit (i.e., detectable molecular densities) of acetone, methanol, ethanol, and ammonia vapors using the *Periodic-90-249 MPS* sensor are 0.125, 1.71, 1.62, and 3.35 nmol/mm^3, respectively, which are denoted by the blue columns in **Figure 7b**. The sensing scheme of MPS device not only recognizes minute concentration changes of VOC with picomolar sensitivity but also exhibits excellent discrimination for different polar VOCs.

3.4 Geometry-dependent sensitivity: micropore size effect

To study the micropore size effect of MPS on the detection sensitivity, the pore number of the MPSs to interact a THz beam is fixed and only the pore width is changed. In **Table 1**, the micropore number of the 23-layered *Periodic-90-249 MPS* is consistent with that of the 6-layered *Periodic-45-133 MPS*, but the pore width of the former device is two times larger than the latter device. These two MPSs are compared to observe the pore-size-dependent sensitivity performance. Similarly,

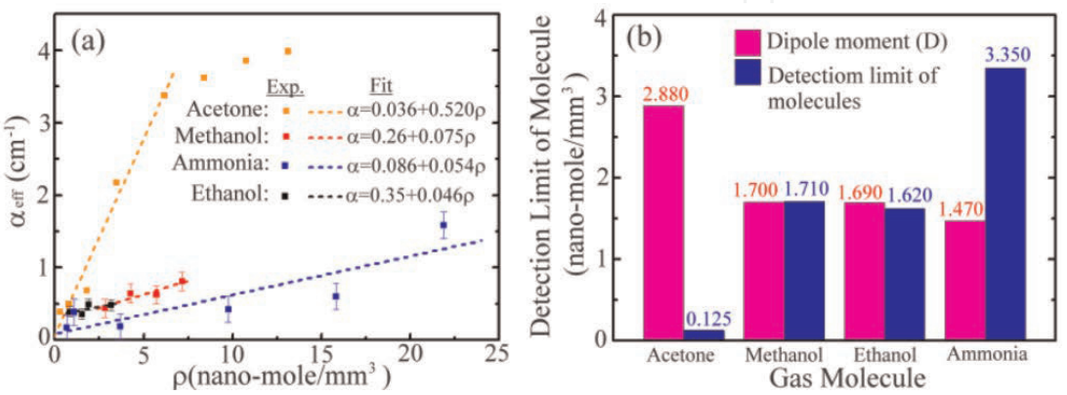

Figure 7.
(a) Detecting the effective absorption coefficients at 0.4 THz under different vapor densities. (b) Investigation of dipole moments and detection limits of the molecular densities (reprinted from Opt. Express 23, 2048-2057 (2015). © 2015 OSA).

the 23-layered *Uniform-90 MPS* and 6-layered *Uniform-45 MPS* devices, having an identical pore number but different pore sizes, are also prepared for this test purpose.

Here is the operation detail to observe the sensitivity dependent on the micropore size effect. The micropore amounts within the THz beam spot for the periodic and uniform MPSs are fixed, and the micropore sizes of both structures are changed to compare their sensitivities in terms of α_{eff} and Δn_{eff}. Regarding the periodic MPS configuration, the small-pore structure (*Periodic-45-133*, average porosity ~37.2%), composed of 6-layered meshes and corresponding to a 0.45 mm thickness, has ~1900 micropores covered by the THz beam. To maintain the same pore quantity in *Periodic-90-249 MPS* (average porosity ~40.5%) under the same THz beam spot, the large-pore mesh of *Periodic-90-249* should be stacked up to 23 layers, corresponding to 3.46 mm thickness. For the MPS uniform configuration, the micropore number covered by the THz beam spot in the 6-layered *Uniform-45 MPS* (porosity ~29.6% and thickness ~0.3 mm) is around 3600. To keep the identical micropore number in the *Uniform-90 MPS* under the same THz beam spot, the *Uniform-90* mesh (i.e., a mesh with the large micropores) with 30.1% porosity should be stacked by 23 layers, corresponding to a 2.3 mm thickness.

The sensitivity of different MPS can be measured by the exposure of the MPS to different VOC amounts, and the THz linear responses in effective absorption and refractive index variation are related to the molecular dipole moment of the VOC (**Figure 7**). In this study, acetone vapor molecule is thus applied as the standard VOC to calibrate the sensitivity performance of MPS because its high dipole moment (~2.88 Debye [33]) is easily perturbed by THz waves. That is, obvious THz electromagnetic attenuation or dispersion can be performed from the acetone vapor molecules. Different amounts of acetone vapor are prepared from different volume concentrations of acetone aqueous solutions, including 2.5, 5, 10, 20, 40, 60, 80, and 100%. All the acetone aqueous solutions are individually loaded inside the microfluidic chamber to naturally evaporate into vapor phase under ambient atmosphere/room temperature until the saturated vapor pressures are approached. The vapor pressure inside the chamber is approximately proportional to the aqueous acetone concentration, following the experiment design in **Figures 4–7**.

Figure 8a and **b** present the α_{eff} and Δn_{eff}, respectively, detected by the *Periodic-45-133* and *Periodic-90-249 MPSs*. In **Figure 8a**, the absorption coefficients in the large (*Periodic-90-249*)—and small (*Periodic-45-133*)-pore MPSs both proportionally increase within a molecular density of about 6 nmol/mm^3 and become saturated at high vapor density. The trace trends of refractive-index variations (Δn_{eff}) shown

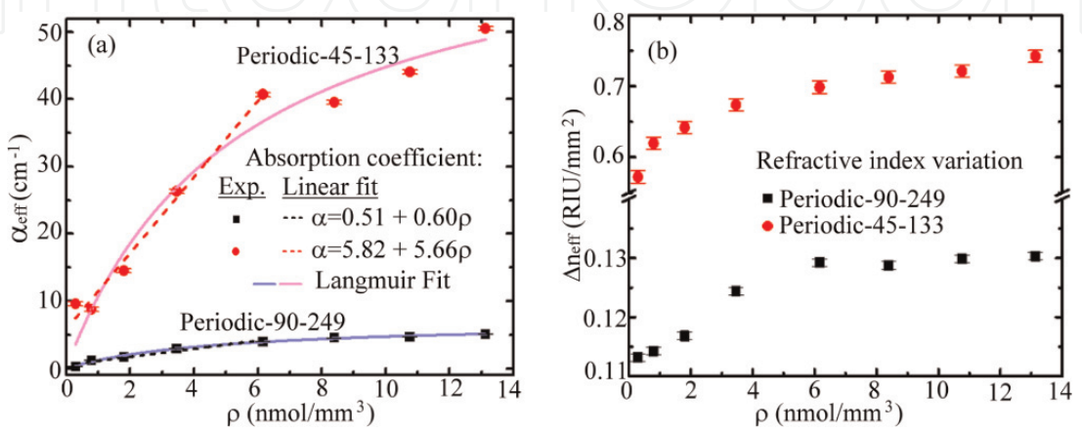

Figure 8.
Detecting (a) effective absorption coefficients and (b) refractive index variations at 0.4 THz within the unit pore volume by the Periodic-45-133 *and* Periodic-90-249 MPSs *(reprinted from Opt. Express 25, 5651-5661 (2017). © 2017 OSA).*

in **Figure 8b** are similar to those of the absorption coefficients (α_{eff}) (**Figure 8a**), except that the saturation phenomenon of Δn_{eff} for the small-pore structure, *Periodic-45-133* MPS, occurs at a much lower vapor density (~2 nmol/mm^3) compared with that of the large-pore structure, *Periodic-90-249* MPS (~6 nmol/mm^3). The comparison results in **Figure 8** show that the α_{eff} and Δn_{eff} of *Periodic-45-133 MPS* for all vapor densities are much larger than those of *Periodic-90-249* MPS. For example, the absorption coefficients of *Periodic-90-249* and *Periodic-45-133 MPSs* (**Figure 8a**) at the vapor molecular density of 13 nmol/mm^3 are around 4 and 50 cm^{-1}, respectively. Further shrinking the micropore volume under a certain vapor density exposure is able to increase the molecular occupied densities, which are confined in the micropore and adsorbed on the pore surface to increase THz wave absorption and phase retardation. The enhancement in α_{eff} and Δn_{eff} of *Periodic-45-133 MPS* is attributed to its small pore size, whereas its pore quantity is identical to that of *Periodic-90-249 MPS*.

The Langmuir adsorption isotherms in **Figure 8a** mean the physisorption of acetone monolayer both occurs on the large and small micropore surfaces of MPS. For the molecular density, <6 nmol/mm^3 (~350 ppm), the THz responsivity of the proportional relation between α_{eff} and ρ in **Figure 8a** are linearly fitted and can be regarded as the sensitive region of the MPS vapor sensor. The α_{eff} of *Periodic-45-133 MPS* increases more rapidly than that of *Periodic-90-249 MPS* within the sensitive region (ρ < 350 ppm). The minimum detectable concentration changes of acetone vapor for the *Periodic-90-249* and *Periodic-45-133 MPS* sensors determined from the system deviation and responsivity slope in **Figure 8** are estimated as less as 108 and 54 pmol/mm^3, corresponding to 6.29 and 3.11 ppm, respectively. The detection limit of *Periodic-45-133 MPS* is two times higher than that of *Periodic-90-249 MPS*, thereby indicating that a decrease in micropore volume (such as half of the pore width) obviously raises the detection sensitivity of the MPS gas sensor.

Figure 9a and **b** show the vapor sensing results of *Uniform-90* and *Uniform-45 MPSs*, respectively. The detected α_{eff} and Δn_{eff} both have linear responsivity versus the vapor density and become saturated at a high vapor density, approximate to the trace trends of the periodic MPSs as shown in **Figure 8**. However, the saturation vapor density of the two uniform MPSs is about 4 nmol/mm^3 (i.e., 200 ppm), and lower than that of the periodic MPSs, which is about 6 nmol/mm^3 or 350 ppm. The THz absorption coefficient curves of *Uniform-90* and *Uniform-45 MPSs* are also well fitted by Langmuir adsorption isotherms with high R^2 values (**Figure 9a**), respectively. According to the slopes of the linear fitting curves in the sensitive region

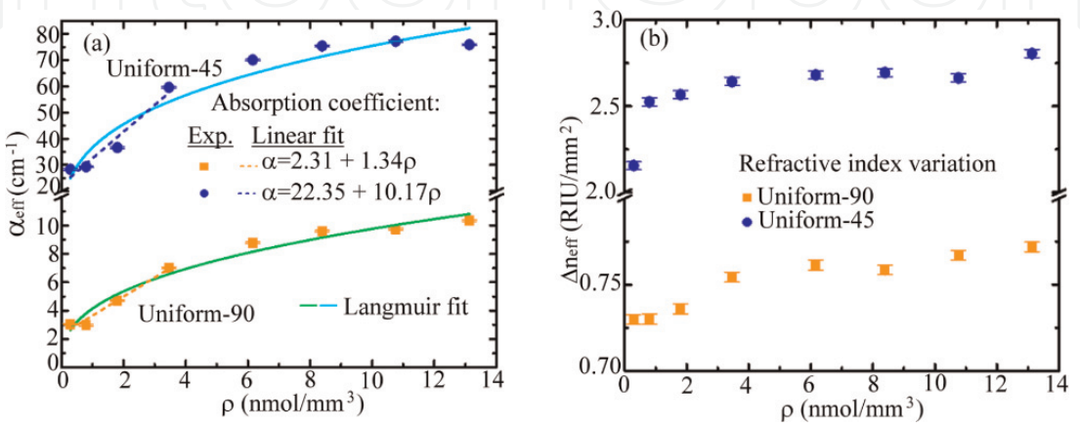

Figure 9.
Detecting (a) effective absorption coefficients and (b) refractive index variations at 0.4 THz within the unit pore volume by the Uniform-45 *and* Uniform-90 MPSs *(reprinted from Opt. Express 25, 5651-5661 (2017). © 2017 OSA).*

(i.e., $\rho < 200$ ppm) and the measurement inaccuracy of the THz absorption coefficient, the minimum detectable concentration changes of acetone vapor using *Uniform-90* and *Uniform-45 MPS* gas sensors are <46 and 31 pmol/mm^3, corresponding to 2.68 and 1.83 ppm, respectively.

The detection sensitivity of *Uniform-45 MPS* is apparently higher than that of *Uniform-90 MPS*, consistent to the comparison result between *Periodic-90-249* and *Periodic-45-133 MPSs*. The performance emphasizes again that half of the pore width, whether periodic or uniform configuration, facilitates the infiltration and adsorption of acetone vapor in the micropores and on the pore surface, leading to an enhanced vapor-field interaction to increase the sensitivity. In addition, the two uniform MPSs in **Figure 9** have obviously higher α_{eff} and Δn_{eff} than those of the periodic MPSs in **Figure 8** under the same vapor density exposure. For example, the largest THz absorption coefficient of *Uniform-45 MPS* is around 80 cm^{-1} and evidently larger than 50 cm^{-1} of *Periodic-45-133 MPS* based on the same 6-layered MPS thickness. The responsivity of linear fitting slopes in **Figures 8** and **9** presents that the two sensing parameters, α_{eff} and Δn_{eff}, of uniform MPSs are increased more rapidly within a narrower sensitive region compared with those of periodic MPSs. It means only fewer amounts of vapor molecules that infiltrate the uniform MPSs can drastically increase the THz absorption coefficient and refractive index variation until the desired chamber saturation is achieved. The average pore width of *Uniform-90/-45 MPS* is smaller than that of *Periodic-90-249/-45-133 MPS* under the similar MPS thickness (i.e., the same stacked layer number of the PET microporous mesh). Therefore, the simple uniform MPS is particularly advantageous for minute vapor sensing with a detection limit of even lower ppm level compared with the periodic MPS.

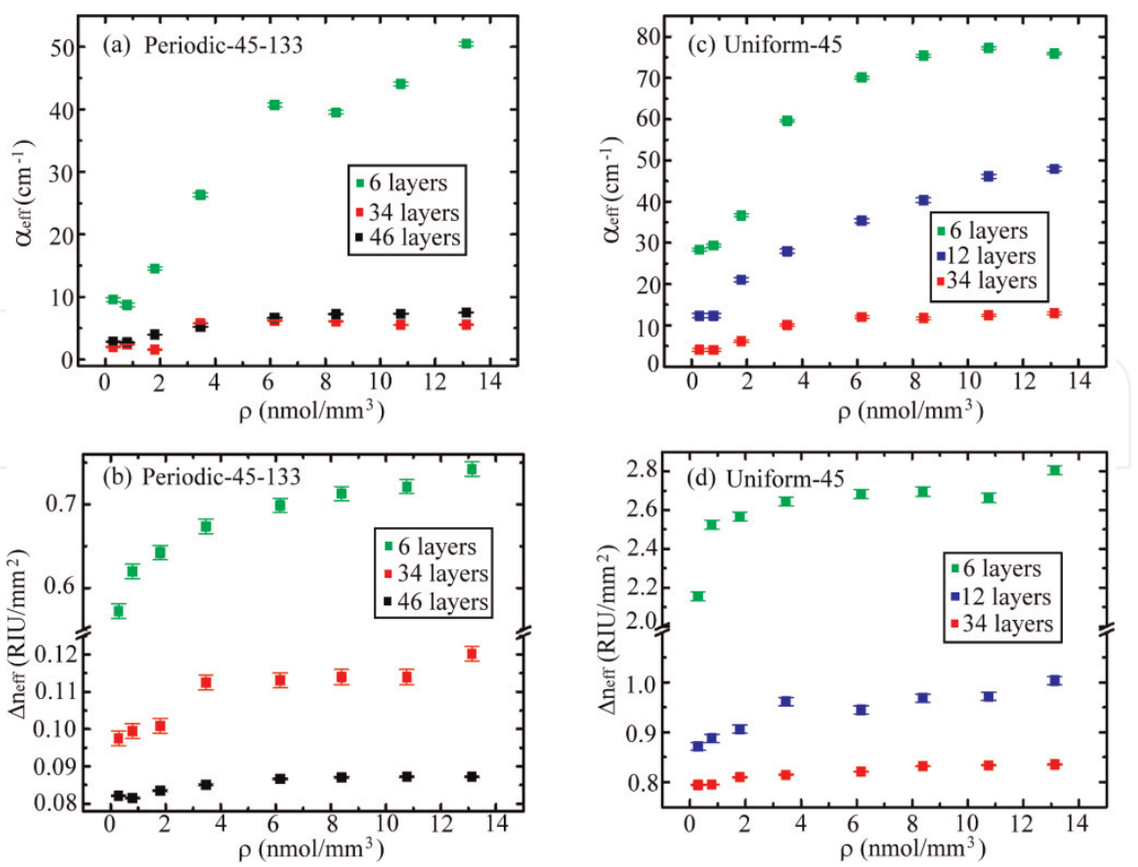

Figure 10.
Detecting (a, c) effective absorption coefficients and (b, d) refractive index variations within unit pore volume by Periodic-45-133 *and* Uniform-45 MPSs *with different thicknesses (reprinted from Opt. Express 25, 5651-5661 (2017). © 2017 OSA).*

3.5 Geometry-dependent sensitivity: micropore number effect

The pore number effect on MPS sensitivity is studied by changing the stacking layer numbers of *Periodic-45-133* and *Uniform-45 MPSs*. As shown in **Table 1**, three different layer numbers of MPSs with identical pore size are prepared for sensitivity comparison in both the *Periodic-45-133* and *Uniform-45 MPSs*. **Figure 10** shows α_{eff} and Δn_{eff} for *Periodic-45-133* and *Uniform-45 MPSs*, which are the small-pore MPSs, respectively, with periodic and uniform configurations. Each type of MPS possesses three kinds of thicknesses formed by stacking different layer numbers of PET mesh. The α_{eff} and Δn_{eff} of *Periodic-45-133 MPS* for 6-layered thickness are evidently larger than those of 34- and 46-layered thicknesses under all vapor densities (**Figure 10a** and **b**). For the response of *Uniform-45 MPS*, both α_{eff} and Δn_{eff} are increased with decreasing device thickness from 34 layers to 12 and 6 layers (**Figure 10c** and **d**). The highest sensitivities for the periodic and uniform MPSs occur in their thinnest conditions (i.e., 6-layered structure). The experiment in this case indicates that the small pore numbers also increase THz wave responses in α_{eff} and Δn_{eff} of the micropores, thereby enhancing the vapor detection sensitivity.

Under a constant amount of vapor exposure, increasing pore quantity or size is equivalent to expanding the pore volume of the microporous structure. The vapor density, congregated within the micropore and adsorbed on the hydrophilic surface, is thus diluted and eventually decreases the measured values in α_{eff} and Δn_{eff}. **Figure 10** also shows that 6-layered *Uniform-45 MPS* requires less acetone vapor amounts to saturate the responsivities of α_{eff} and Δn_{eff} because of its less micropore volume/number, comparing to those of 12- or 34-layered *Uniform-45 MPS*. The vapor saturation density of 6-layered *Uniform-45 MPS* occurs at around 4 nmol/mm^3 (i.e., 200 ppm), indicating the dynamic range of linear responsivity is sufficiently wide for minute vapor detection.

3.6 Sensing applications

The micropore size dependent sensitivity of the four types of MPSs is summarized in **Table 2**, where the sensitivity corresponds to the slope of linear fit. The blank chamber represents the vapor sensing performance of the microfluidic chamber without the MPS. It is THz vapor sensing in the free space measured by traditional THz-TDS. The *Uniform-45 MPS* with a 6-layered thickness has the highest sensitivity, down to 1 ppm-level acetone vapor molecule. Such the sensitivity is more excellent than that of the 23-layered *Periodic-90-249 MPS* and much higher than that of blank chamber.

MPS No.	Layer number	Error bar at 0.4 THz (cm^{-1})	Sensitivity (cm^{-1}/nmol mm^{-3})	Detection limit (ppm)
Periodic-90-249	23	0.065	0.60	6.288
Periodic-45-133	6	0.303	5.66	3.105
Uniform-90	23	0.062	1.34	2.683
Uniform-45	6	0.320	10.17	1.825
Blank chamber	0	0.007	0.013	32.37

Reprinted from Opt. Express 25, 5651-5661 (2017). © 2017 OSA.

Table 2.
Sensing performance of MPS for acetone vapor detection.

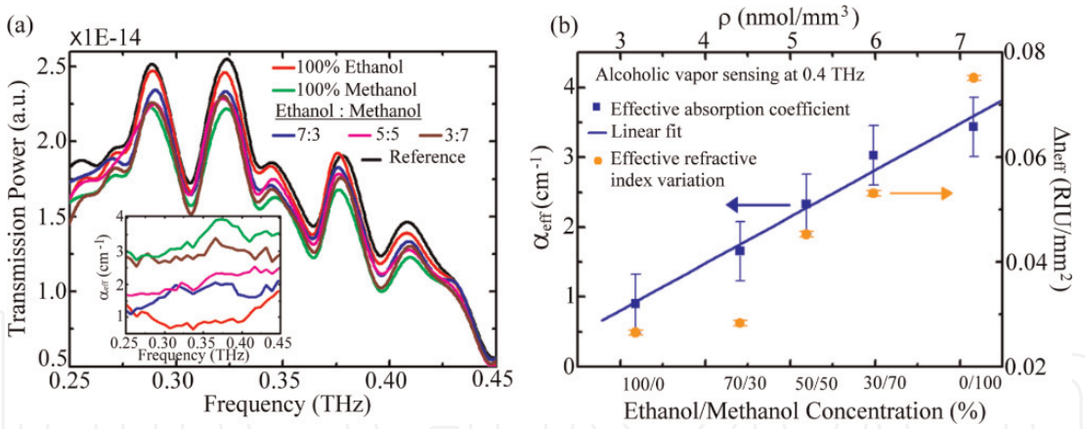

Figure 11.
(a) THz-wave transmission spectrum for sensing toxic methanol adulterated in alcoholic solutions: (inset) detecting THz absorption coefficient spectra by the 6-layered Unifrom-45 *MPS. (b) Detecting absorption coefficient and refractive index variation versus different concentrations of adulterated alcoholic aqueous solutions at 0.4 THz (reprinted from Opt. Express 25, 5651-5661 (2017). © 2017 OSA).*

The 6-layered *Uniform-45 MPS* can thus be used for identifying toxic methanol adulterated in alcoholic solutions. Adulterated alcoholic solutions are prepared by mixing different volume ratios of methanol with ethanol, including 1:0, 7:3, 5:5, 3:7, and 0:1 (ethanol/methanol). The adulterated alcoholic solution is injected into the microfluidic channel of the sealed microfluidic chamber, as shown in **Figure 3c**, and becomes the vapor molecules via natural evaporation to be detected by THz waves. **Figure 11a** illustrates the THz transmission spectrum of *Uniform-45 MPS* exposed to the vaporized mixtures, which are generated from various concentrations of adulterated alcoholic solutions. THz transmission power apparently decreases in the frequency range of 0.25–0.45 THz as the volume ratio of methanol increases. The THz absorption coefficient spectra for the different concentrations of adulterated alcoholic vapors can be estimated and shown in the inset of **Figure 11a**. The measured THz absorption coefficients for each concentration of alcoholic vapor are almost constant in the frequency range of 0.25–0.45 THz. The relatively high absorption coefficients are resulted from the increment of the adulterated methanol concentration. The refractive index variation before and after exposure to different concentrations of alcoholic vapors can also be calculated. **Figure 11b** plots the relations of the α_{eff} and Δn_{eff} at 0.4 THz against different concentrations of alcoholic aqueous solutions. The α_{eff} and Δn_{eff} increase with the methanol concentration adulterated in the alcoholic solution. The proportional relation of α_{eff} and ρ is linearly fitted as $\alpha_{eff} = 1.2 + 0.67\rho$. The sensing result of **Figure 11** reveals that the colorless and high THz-absorbed alcoholic aqueous solutions with different concentrations of toxic methanol adulteration can be easily distinguished using the MPS gas sensor composed of 6-layered *Uniform-45 MPS*.

4. Conclusions

Optical gas sensors are experimentally demonstrated using the THz refractive indices and THz absorption coefficients when THz waves propagating through the dielectric-layer media are monitored in a spectroscopic system (THz-TDS). The cylindrical layer is applied from a glass dielectric pipe to be the waveguide resonator. Based on the FP criteria and FDTD simulation, the THz frequency of pipe-waveguide resonance field is approximately proportional to the refractive index of the pipe core. The experimental results present that only the high-order

resonant modes are sensitive to the refractive-index variation due to the high evanescent power toward the pipe core. Different analytes with different vapor pressures, such as water, HCl, acetone and ammonia, are thus identified by a pipe-waveguide resonator. To further improve the detection sensitivity and selectivity, the MPS structures are applied as 1 THz artificial material to adsorb vapor molecules. THz absorption coefficients of the unit volume are defined based on the effective medium concept and demonstrated to identify various vapor molecules in the investigation. The molecular dipole moment dominates THz absorption in the unit volume of micropore when several analytes, such as the acetone, methanol, ethanol and ammonia, are test in one MPS sensor. The sensing performance based on the MPS geometry is studied for the sensitivity and the possible detection limit. For the acetone molecule, the 6-layered *Uniform-45 MPS* sensor has the high sensitivity and the detection limit is potentially down to 1.8 ppm. The 6-layered *Uniform-45 MPS* sensor is eventually applied for one sensing application to distinct methanol and ethanol vapor molecules from various liquid mixtures. The MPS sensing scheme is therefore applicable to realize one optical gas sensor.

Acknowledgements

This work was supported by grants-in-aid for scientific research from the Ministry of Science and Technology of Taiwan (MOST 107-2221-E-006-183-MY3) and Japan Society for the Promotion of Science (JSPS, KAKENHI, JP16K17525).

Author details

Borwen You[1] and Ja-Yu Lu[2*]

1 Department of Applied Physics, Faculty of Pure and Applied Sciences, University of Tsukuba, Tsukuba, Ibaraki, Japan

2 Department of Photonics, National Cheng Kung University, Tainan, Taiwan

*Address all correspondence to: jayu@mail.ncku.edu.tw

References

[1] Spanel P, Smith D. Selected ion flow tube: A technique for quantitative trace gas analysis of air and breath. Medical & Biological Engineering & Computing. 1996;**34**:409

[2] Phillips M, Herrera J, Krishnan S, Zain M, Greenberg J, Cataneo RN. Variation in volatile organic compounds in the breath of normal humans. Journal of Chromatography B. 1999;**729**:75

[3] Fosnight AM, Moran BL, Medvedev IR. Chemical analysis of exhaled human breath using a terahertz spectroscopic approach. Applied Physics Letters. 2013; **103**:133703

[4] Kanan SM, El-Kadri OM, Abu-Yousef IA, Kanan MC. Semiconducting metal oxide based sensors for selective gas pollutant detection. Sensors-Basel. 2009;**9**:8158-8196

[5] Wang L, Kalyanasundaram K, Stanacevic M, Goum P. Nanosensor device for breath acetone detection. Sensor Letters. 2010;**8**:1-4

[6] Chang SJ, Hsueh TJ, Chen IC, Hsieh SF, Chang SP, Hsu CL, et al. Highly sensitive ZnO nanowire acetone vapor sensor with Au adsorption. IEEE Transactions on Nanotechnology. 2008; **7**:754-759

[7] Chu R, Guan C, Bo Y, Shi J, Zhu Z, Li P, et al. All-optical graphene-oxide humidity sensor based on a side-polished symmetrical twin-core fiber Michelson interferometer. Sensors and Actuators B: Chemical. 2019;**284**: 623-627

[8] Romanovskii OA, Sadovnikov SA, Kharchenko OV, Yakovlev SV. Development of near/mid IR differential absorption OPO lidar system for sensing of atmospheric gases. Optics and Laser Technology. 2019;**116**: 43-47

[9] Kanawade R, Kumar A, Pawar D, Vairagi K, Late D, Sarkar S, et al. Negative axicon tip-based fiber optic interferometer cavity sensor for volatile gas sensing. Optics Express. 2019;**27**: 7277-7290

[10] Mittleman D. Sensing with Terahertz Radiation. Heidelberg, Berlin: Springer-Verlag; 2003. pp. 39-115

[11] Mittleman DM, Jacobsen RH, Neelamani R, Baraniuk RG, Nuss MC. Gas sensing using terahertz time domain spectroscopy. Applied Physics B: Lasers and Optics. 1998;**67**:379-390

[12] Gerecht E, Douglass KO, Plusquellic DF. Chirped-pulse terahertz spectroscopy for broadband trace gas sensing. Optics Express. 2011;**19**: 8973-8984

[13] Lin H, Withayachumnankul W, Fischer BM, Mickan SP and Abbott D. Gas recognition with terahertz time-domain spectroscopy and spectral catalog: a preliminary study. In: Proceedings SPIE 2008; Terahertz Photonics; 68400X. DOI: 10.1117/ 12.760558

[14] Melinger JS, Yang Y, Mandehgar M, Grischkowsky D. THz detection of small molecule vapors in the atmospheric transmission windows. Optics Express. 2012;**20**:6788-6807

[15] Bigourd D, Cuisset A, Hindle F, Matton S, Bocquet R, Mouret G, et al. Multiple component analysis of cigarette smoke using THz spectroscopy, comparison with standard chemical analytical methods. Applied Physics B: Lasers and Optics. 2007;**86**: 579-586

[16] Neese CF, Medvedev IR, Plummer GM, Frank AJ, Ball CD, De Lucia FC. Compact submillimeter/terahertz gas

sensor with efficient gas collection, preconcentration, and ppt sensitivity. IEEE Sensors Journal. 2012;**12**:2565

[17] Consolino L, Bartalini S, Beere HE, Ritchie DA, Vitiello MS, De Natale P. THz QCL-based cryogen-free spectrometer for in situ trace gas sensing. Sensors-Basel. 2013;**13**: 3331-3340

[18] Chen T, Han Z, Liu J, Hong Z. Terahertz gas sensing based on a simple one-dimensional photonic crystal cavity with high-quality factors. Applied Optics. 2014;**53**:3454-3458

[19] Benz A, Deutsch C, Brandstetter M, Andrews AM, Klang P, Detz H, et al. Terahertz active photonic crystals for condensed gas sensing. Sensors-Basel. 2011;**11**:6003

[20] Lai CH, Hsueh YC, Chen HW, Huang YJ, Chang HC, Sun CK. Low-index terahertz pipe waveguides. Optics Letters. 2009;**34**:3457

[21] Litchinitser NM, Abeeluck AK, Headley C, Eggleton BJ. Antiresonant reflecting photonic crystal optical waveguides. Optics Letters. 2002;**27**: 1592-1594

[22] You B, Lu JY, Yu CP, Liu TA, Peng JL. Terahertz refractive index sensors using dielectric pipe waveguides. Optics Express. 2012;**20**: 5858-5866

[23] Dean JA. Lange's Handbook of Chemistry. McGraw-Hill Professional; 1999. Chapter 5

[24] Washburn EW. International Critical Tables of Numerical Data, Physics, Chemistry and Technology. Vol. IV. Knovel; 2003

[25] Yang Y, Shutler A, Grischkowsky D. Measurement of the transmission of the atmosphere from 0.2 to 2 THz. Optics Express. 2011;**19**:8830-8838

[26] Petrucci RH. General Chemistry: Principles and Modern Applications. Pearson Prentice Hall; 2007

[27] Beare WG, McVicar GA, Ferguson JB. The determination of vapor and liquid compositions in binary systems. The Journal of Physical Chemistry. 1929; **34**:1310-1318

[28] Zhang J, Grischkowsky D. Terahertz time-domain spectroscopy study of silica aerogels and adsorbed molecular vapors. The Journal of Physical Chemistry. B. 2004;**108**:18590-18600

[29] Shi W, Ding YJ. Fingerprinting molecules based on direct measurement of absorption spectrum by frequency-tuning monochromatic THz source. Laser Physics Letters. 2004;**1**:560-564

[30] Xu P, Yu H, Li X. Functionalized mesoporous silica for microgravimetric sensing of trace chemical vapors. Analytical Chemistry. 2011;**83**: 3448-3454

[31] Xie Z, Cao K, Zhao Y, Bai L, Gu L, Xu H, et al. An optical nose chip based on mesoporous colloidal photonic crystal beads. Advanced Materials. 2014;**26**:2413-2418

[32] Nelson RD, Lide DR and Maryott AA. Selected values of electric dipole moments for molecules in the gas phase. U. S. National Bureau of Standards NSRDS-NBS; 1967. 10

[33] Dorosh O, Kisiel Z. Electric dipole moments of acetone and of acetic acid measured in supersonic expansion. Acta Physica Polonica A. 2007;**112**:S95-S104